

Article

N, S, P-Codoped Graphene-Supported Ag-MnFe₂O₄ Heterojunction Nanoparticles as Bifunctional Oxygen Electrocatalyst with High Efficiency

Hongzhou Dong¹, Yingjie Chen^{1,*}, Chong Gong¹, Lina Sui¹, Qiong Sun¹, Kangle Lv^{2,*}  and Lifeng Dong^{1,3,*}

¹ College of Materials Science and Engineering, Qingdao University of Science and Technology, Qingdao 266042, China; dhz1001@qust.edu.cn (H.D.); gcsd97427@126.com (C.G.); linasui@qust.edu.cn (L.S.); sunqiong@qust.edu.cn (Q.S.)

² College of Resources and Environmental Science, South-Central University for Nationalities, Wuhan 430074, China

³ Department of Physics, Hamline University, St. Paul, MN 55104, USA

* Correspondence: chenyingjie@qust.edu.cn (Y.C.); lvkangle@mail.scuec.edu.cn (K.L.); donglifeng@qust.edu.cn (L.D.)

Abstract: Due to slow kinetics of oxygen reduction reaction (ORR) and oxygen evolution reaction (OER) during discharging and charging processes, it is essential to rationally design and synthesize non-precious metal bifunctional electrocatalysts with good performance for metal-air batteries. Herein, Ag-MnFe₂O₄ heterojunction nanoparticles supported on N, S, P-codoped graphene (NSPG) are developed with enhanced ORR and OER bifunctional electrocatalytic activities and stability. In contrast, S, P-doped graphene (SPG) and N, P-doped graphene (NPG) show less stabilization for the heterojunction particles. For example, under alkaline conditions, the ORR half-wave potential of Ag-MnFe₂O₄/NSPG can reach 0.831 V, and the over potential for OER is 0.56 V at the current density 10 mA·cm⁻². Furthermore, Ag-MnFe₂O₄/NSPG shows better methanol resistance and durability than Pt/C catalysts.

Keywords: bifunctional; graphene; electrocatalyst; MnFe₂O₄



Citation: Dong, H.; Chen, Y.; Gong, C.; Sui, L.; Sun, Q.; Lv, K.; Dong, L. N. S, P-Codoped Graphene-Supported Ag-MnFe₂O₄ Heterojunction Nanoparticles as Bifunctional Oxygen Electrocatalyst with High Efficiency. *Catalysts* **2021**, *11*, 1550. <https://doi.org/10.3390/catal11121550>

Academic Editors: Marc Cretin, Sophie Tingry and Zhenghua Tang

Received: 24 November 2021

Accepted: 10 December 2021

Published: 19 December 2021

Publisher's Note: MDPI stays neutral with regard to jurisdictional claims in published maps and institutional affiliations.



Copyright: © 2021 by the authors. Licensee MDPI, Basel, Switzerland. This article is an open access article distributed under the terms and conditions of the Creative Commons Attribution (CC BY) license (<https://creativecommons.org/licenses/by/4.0/>).

1. Introduction

Design and synthesis of efficient bifunctional oxygen electrocatalysts are of critical importance but challenging for large-scale implementations of Zn-air batteries [1]. Recently, silver and metal oxides were reported as potential alternative candidates for Pt-based catalysts [2,3]. After loading onto carbon supports, these relatively inexpensive candidates can promote both oxygen reduction reaction (ORR) and oxygen evolution reaction (OER). The combination of silver and metal oxide nanocrystals can improve their electrical conductivity and bifunctional activity due to direct or indirect coupling and electron transfer between them. For example, the combination of Mn-oxides with Fe, N-codoped carbon can scavenge hydrogen peroxide for ORR [4]. Different methods have been established to synthesize N-doped carbon materials from CO₂ [5] and biomass materials [6]. An increased surface nitrogen content was identified as one of the reasons for excellent activity [7]. However, the volume-specific activity and electronic conductivity of these candidates still need to be improved.

Graphene (G) has been explored as non-metal catalyst and support for electrochemical reactions. Pristine graphene has no catalytic activity [8], but chemical doping of heteroatoms into graphene lattices could transfer nearby carbon atoms into “active sites”. Additionally, defects including single C atom vacancy, Stone-Wales defects, and grain boundaries can modify electronic structures [9]. For example, sole-doped carbons, dual-doped carbons (N/S [10,11], N/B [12], and N/P [13,14]), and triple-doped carbon materials (N/P/S [15]) demonstrated improved electrochemical properties. The introduction of N

and/or S atoms could increase spin polarization and charge density of adjacent carbon atoms to enhance electrocatalytic activities [16,17]. P-doped graphene could provide active sites to facilitate the formation and dissociation of OOH, the rate-limiting step of ORR [18]. Furthermore, dual-doped and tri-doped graphene demonstrates even better performances as an electrocatalyst than single-doped graphene due to synergetic effects among different heteroatoms [9,19]. However, catalytic activities of doped graphene are still not comparable to Pt/C.

In addition, these doped graphene can also be utilized to support and stabilize metal-containing catalysts. According to the hard-soft-acid-base theory, the binding ability of hard base decreases along with its reducing electro-negativity [20]. Generally, silver is a soft acid [21], while sulfur is a soft base. The affinity interaction between silver and sulfur helps stabilize the heterostructure of catalysts. Similarly, the affinity interaction between iron and nitrogen in carbon materials improves the performance of oxygen electrocatalysts [22,23]. There are various bifunctional catalysts, including Co_3O_4 @ graphene [24], Co_3O_4 /N-doped graphene [25], and CoFe_2O_4 /graphene aerogel [26]. Graphene supports are believed to promote electron transfer and facilitate mass transport of reactants to electrocatalysts. It is possible to boost the performances of metal heterojunction particle electrocatalysts by the supporting of multi-doped graphene.

Herein, S, P-co-doped graphene (SPG), N, P-co-doped graphene (NPG), and N, S, P-multi-doped graphene (NSPG) are synthesized and utilized as supports for $\text{Ag-MnFe}_2\text{O}_4$ heterojunction nanoparticles. Compared with SPG and NPG, NSPG shows better stabilization for the heterojunction structure. As a result, $\text{Ag-MnFe}_2\text{O}_4$ /NSPG demonstrates better electrocatalytic performance and higher catalytic activity for ORR and OER.

2. Results and Discussion

XRD analyses were conducted to identify crystallographic structures of carbon-based materials and transition metal oxide NPs. As shown in Figure 1a, there is a typical diffraction peak around 26° , corresponding to the (002) plane of graphene. It indicates that various oxygen-containing functional groups on graphene oxide disappear to form graphene after calcination [27], and NPG, SPG, and NSPG have good structures. The XRD patterns of $\text{Ag-MnFe}_2\text{O}_4$ /NPG, $\text{Ag-MnFe}_2\text{O}_4$ /SPG, and $\text{Ag-MnFe}_2\text{O}_4$ /NSPG (Figure 1b) display diffraction features of Ag (JCPDS 65-2871) and MnFe_2O_4 (JCPDS 10-0319). The peaks at 38.1° , 44.3° , and 64.5° correspond to the (111), (200) and (220) planes of Ag, respectively [28].

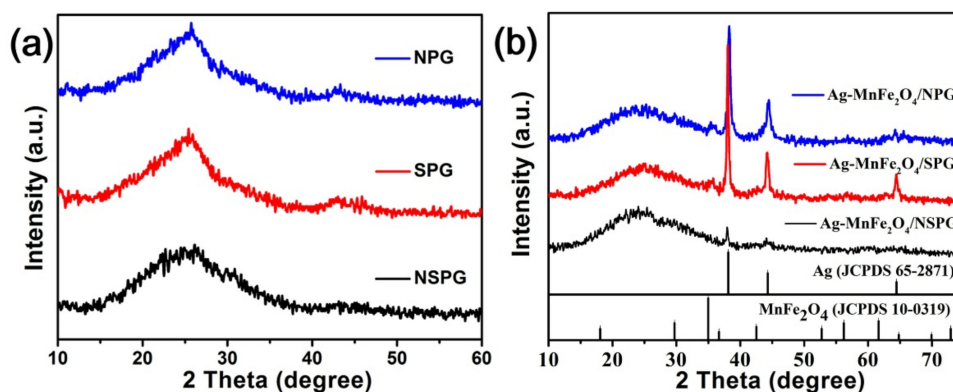


Figure 1. (a) XRD patterns of NPG, SPG and NSPG. (b) XRD patterns of $\text{Ag-MnFe}_2\text{O}_4$ /NPG, $\text{Ag-MnFe}_2\text{O}_4$ /SPG and $\text{Ag-MnFe}_2\text{O}_4$ /NSPG.

Raman spectra of $\text{Ag-MnFe}_2\text{O}_4$ /NPG, $\text{Ag-MnFe}_2\text{O}_4$ /SPG, and $\text{Ag-MnFe}_2\text{O}_4$ /NSPG are shown in Figure 2. The D bands around 1350 cm^{-1} are associated with the sp^3 defect sites, while the G bands near 1600 cm^{-1} represent the bond stretching of sp^2 -bonded pairs [10]. The I_D/I_G ratios for $\text{Ag-MnFe}_2\text{O}_4$ /NPG, $\text{Ag-MnFe}_2\text{O}_4$ /SPG, and $\text{Ag-MnFe}_2\text{O}_4$ /NSPG

$\text{MnFe}_2\text{O}_4/\text{NSPG}$ are 0.99, 0.99, 1.01, respectively. It indicates similar defect features for NPG, SPG, and NSPG.

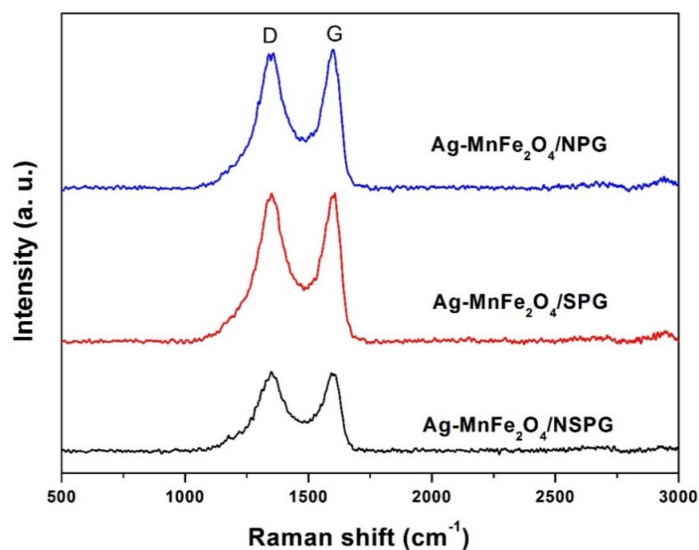


Figure 2. Raman spectra of $\text{Ag-MnFe}_2\text{O}_4/\text{NPG}$, $\text{Ag-MnFe}_2\text{O}_4/\text{SPG}$, and $\text{Ag-MnFe}_2\text{O}_4/\text{NSPG}$.

The elemental mapping images of NSPG exhibit the stacking of curved graphene layers (Figure 3) and C (red), N (green), P (bright yellow), O (orange), and S (blue) elements are uniformly distributed on the NSPG surface. Thus, N, S, and P elements are successfully doped into graphene.

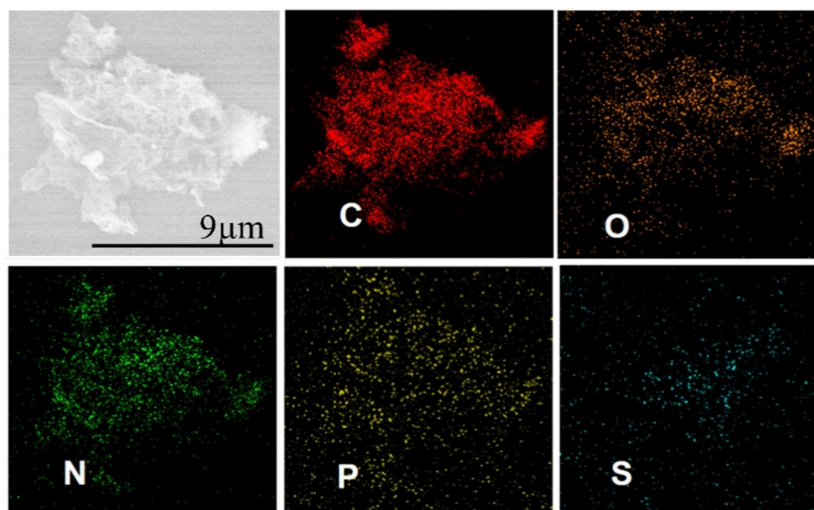


Figure 3. EDS elemental mapping images of NSPG.

TEM images in Figure 4 exhibit that heterogeneous nanoparticles are uniformly dispersed on the doped graphene sheets, which can facilitate electron transport during catalytic processes and more exposure of active sites, thereby enhancing catalytic performances of the catalyst. There is no obvious aggregation of $\text{Ag-MnFe}_2\text{O}_4$ nanoparticles on the supports, indicating successful loading of nanoparticles on doped graphene. Interestingly, the size of Ag nanocomposites on different supports showed small differences. The average size of Ag nanocrystals in $\text{Ag-MnFe}_2\text{O}_4/\text{NSPG}$ is near 8 nm, while those for $\text{Ag-MnFe}_2\text{O}_4/\text{NPG}$ and $\text{Ag-MnFe}_2\text{O}_4/\text{SPG}$ are near 11 nm. It is proved that various doping elements have different effects on metal particles.

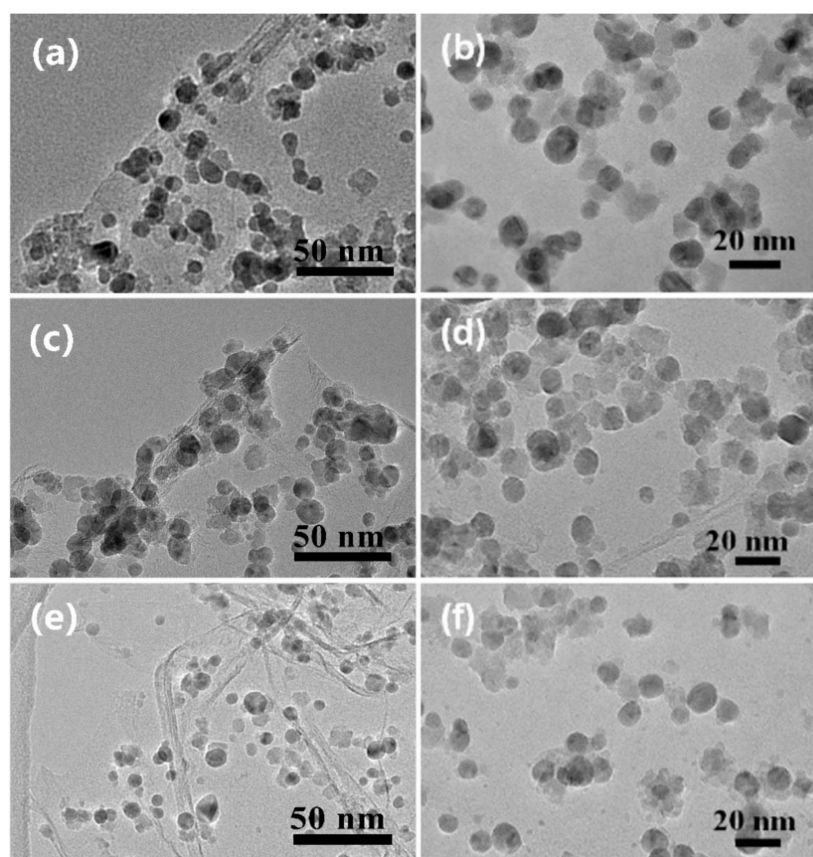


Figure 4. TEM images for (a,b) Ag-MnFe₂O₄/NPG, (c,d) Ag-MnFe₂O₄/SPG, and (e,f) Ag-MnFe₂O₄/NSPG.

XPS survey spectra in Figure 5a show the presence of doping elements and loading nanoparticles. As given in Figure 5b,c the bonds of N 1s (Pyridinic N: 398.32 eV) and S 2p (S 2P_{1/2}: 165.23 eV) of Ag-MnFe₂O₄/NSPG have slightly negative shift than N 1s (Pyridinic N: 398.58 eV) of Ag-MnFe₂O₄/NPG and S 2p (S 2P_{1/2}: 165.31 eV) of Ag-MnFe₂O₄/SPG, and the sharpness of the peak shape slightly decreases. From Table 1, the contents of N 1s and S 2p in Ag-MnFe₂O₄/NSPG are lower than N 1s in Ag-MnFe₂O₄/NPG and S 2p in Ag-MnFe₂O₄/SPG, respectively. Doping elements and metal nanoparticles can provide defect locations, and electron transfer between them can offer large number of ORR catalytically active sites to easily adsorb oxygen and greatly improve catalytic activity [29]. In addition, the combination of N and Fe and the effect of doping P on C and N have been shown to improve the ORR activity. Therefore, Ag-MnFe₂O₄/NSPG can have higher catalytic activities than other samples.

Table 1. Elemental contents determined by XPS.

Samples	Content (at. %)						
	N 1s	S 2p	P 2p	C 1s	Ag 3d	Mn 2p	Fe 2p
Ag-MnFe ₂ O ₄ /NPG	2.65	/	0.89	91.38	1.59	1.25	2.24
Ag-MnFe ₂ O ₄ /SPG	/	2.55	0.86	91.85	1.53	1.28	1.93
Ag-MnFe ₂ O ₄ /NSPG	1.65	1.72	0.93	90.92	1.48	1.22	2.08

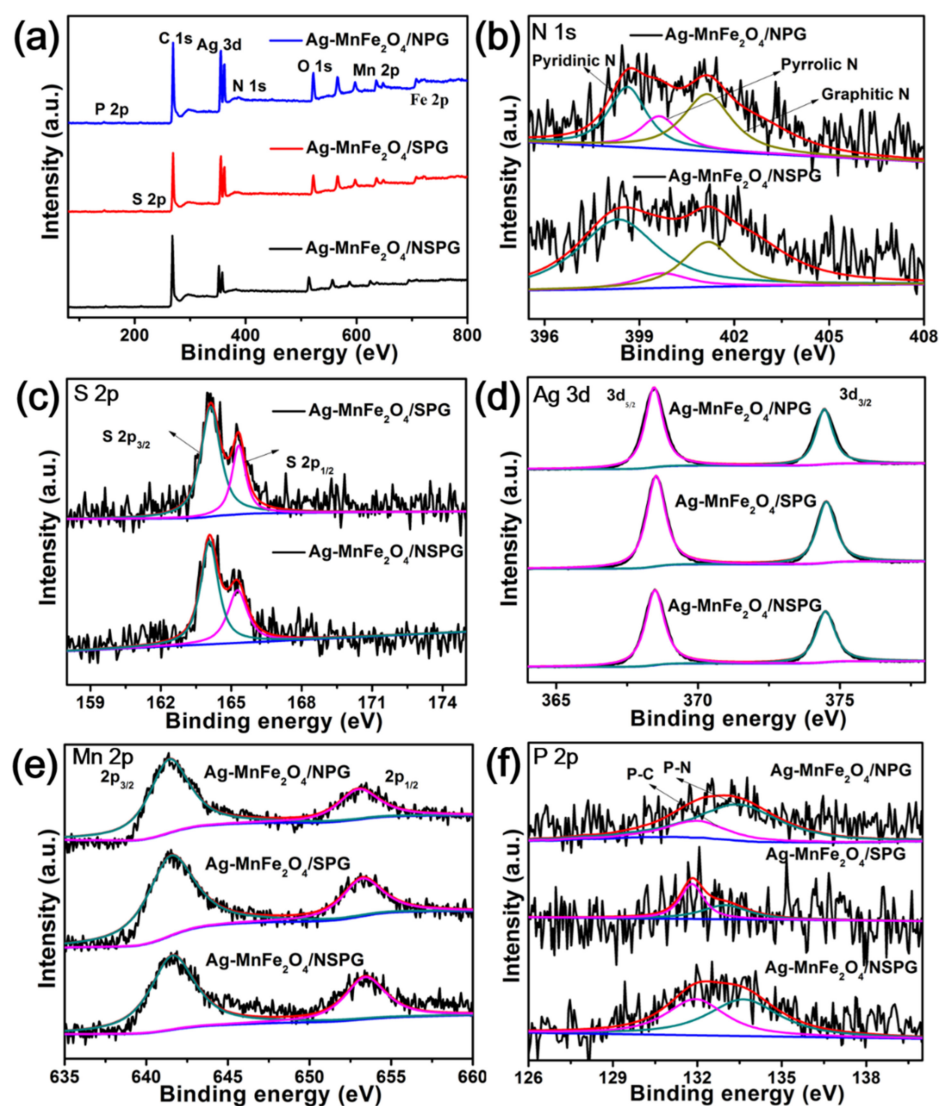


Figure 5. (a) XPS survey spectra and corresponding high-resolution spectra of (b) N 1s, (c) S 2p, (d) Ag 3d, (e) Mn 2p, and (f) P 2p.

For the determination of the bulk content of Ag, Mn, and Fe in the synthesized catalysts, ICP-OES was used. Elemental concentrations are given in Table 2. The atom ratios of Ag: Mn: Fe were, respectively, 1:1.01:1.83, 1:1.11:1.79, and 1:1.09:1.79 in Ag-MnFe₂O₄/NPG, Ag-MnFe₂O₄/SPG, and Ag-MnFe₂O₄/NSPG, and the loading contents of Ag-MnFe₂O₄ were 22.02 wt.%, 21.61 wt.%, 22.13 wt.%, respectively.

Table 2. Concentrations of Ag, Mn, and Fe determined by ICP-OES.

	Elemental Concentration (ppm)		
	Ag	Mn	Fe
Ag-MnFe ₂ O ₄ /NPG	183.5	94.3	173.6
Ag-MnFe ₂ O ₄ /SPG	177.9	100.4	164.8
Ag-MnFe ₂ O ₄ /NSPG	182.8	101.6	169.4

To evaluate ORR catalytic performances of obtained composites, cyclic voltammetry (CV), and linear sweep voltammetry (LSV) measurements were performed in O₂- or N₂-saturated 0.1 M KOH solution using a rotating disk electrode (RDE). Some important data of ORR catalytic performances are shown in Table 3. Figure 6a shows CVs of the three

samples to explore their ORR catalytic activities. There are obvious reduction peaks appear for catalysts in O_2 -saturated electrolyte. The reduction peaks between 0.80 V and 1.10 V correspond to the reduction of AgO to Ag, while the peaks in the range of 0.60 V to 0.80 V are assigned to ORR catalytic activities. The ORR peak potentials of Ag-MnFe₂O₄/NSPG (0.775 V) is more positive than that of Ag-MnFe₂O₄/SPG (0.733 V) and Ag-MnFe₂O₄/NPG (0.723 V). The results show that Ag-MnFe₂O₄/NSPG and Ag-MnFe₂O₄/SPG have good electrocatalytic properties. To get further insight into ORR activities, LSVs of the samples with the same scan rate (5 mV s⁻¹) and rotating speed (1600 rpm) are shown in Figure 6b. Onset potential of Ag-MnFe₂O₄/NSPG (0.887 V) is better than those of Ag-MnFe₂O₄/SPG (0.871 V), Ag-MnFe₂O₄/NPG (0.869 V), and commercial Pt/C (0.879 V). A similar trend is observed in half-wave potentials. Ag-MnFe₂O₄/NSPG presents as of 0.831 V, more positive than Ag-MnFe₂O₄/SPG (0.769 V), Ag-MnFe₂O₄/NPG (0.741 V) and Pt/C (0.827 V), indicating that Ag-MnFe₂O₄/NSPG has superior ORR activities. As reported, Ag-MnFe₂O₄ nanoparticles supported on N, S-co-doped graphene was detected to be 0.824 V of half-wave potential in LSV [30]. This clearly shows that the doping of graphene with N, S, and P can significantly improve electrocatalytic activities of Ag-MnFe₂O₄ toward ORR. Co-doping of NS, NP, SP, or NSP in graphene can produce asymmetric spin or charge density, resulting in more active sites and higher catalytic activity than single doping catalysts [31]. The results also show that NSPG can significantly improve electrocatalytic performances of Ag-MnFe₂O₄. The electrocatalytic performances of different catalysts are shown in Figure 7.

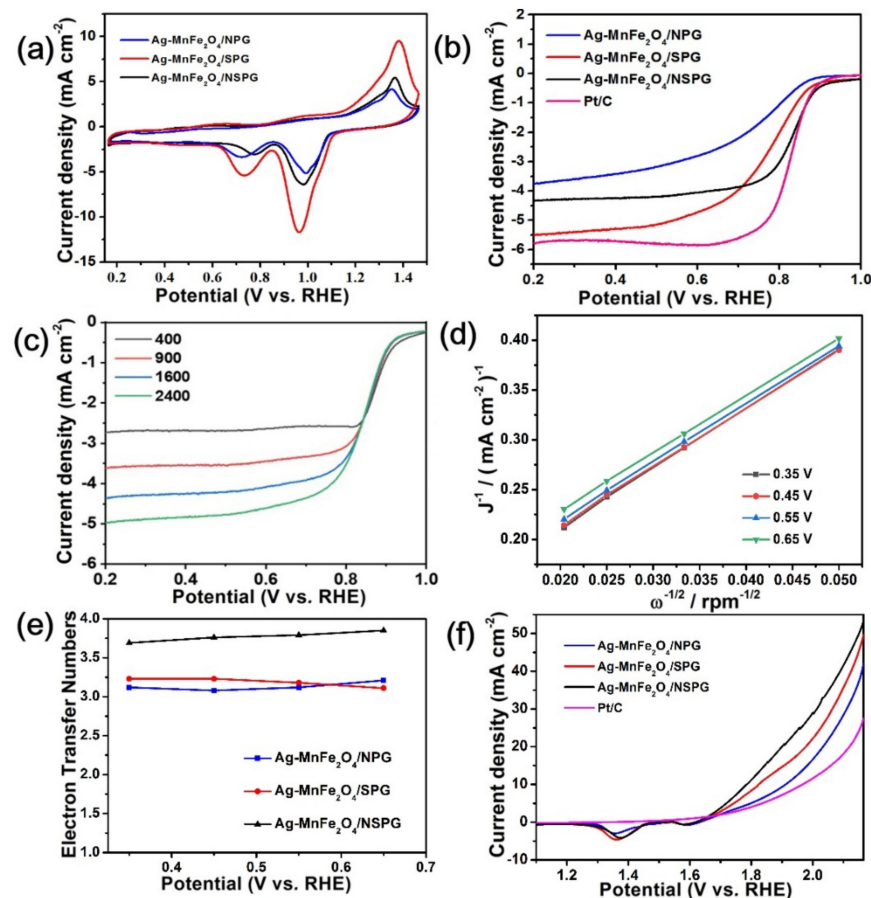
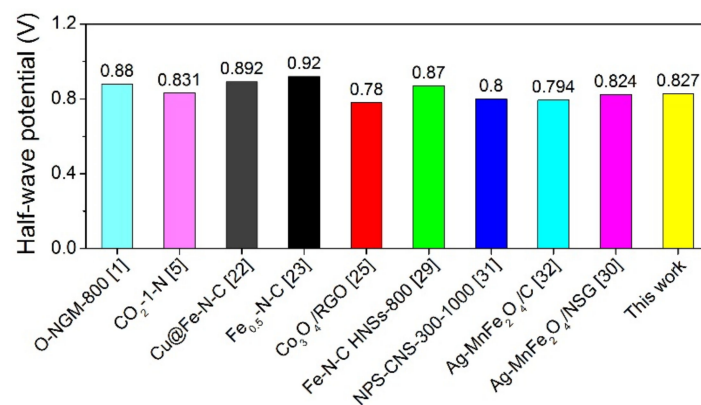


Figure 6. (a) CV and (b) LSV curves of the three samples. (c) ORR polarization curves of Ag-MnFe₂O₄/NSPG at different rotation rates and their corresponding (d) K-L plots and (e) *n* values in comparison to two other samples. (f) OER LSV curves of the three samples and Pt/C.

Table 3. ORR catalytic performances of the three samples.

	Peak Potentials(V) in CV	Onset Potential(V) in LSV	Half-Wave Potential(V) in LSV
Ag-MnFe ₂ O ₄ /NPG	0.723	0.869	0.741
Ag-MnFe ₂ O ₄ /SPG	0.733	0.871	0.769
Ag-MnFe ₂ O ₄ /NSPG	0.775	0.887	0.831
Pt/C	/	0.879	0.827

In order to clarify redox kinetic characteristics and catalytic pathway of Ag-MnFe₂O₄/NSPG, LSV measurements were conducted (Figure 6c). Limit current density rises with increasing electrode rotation rate, enabling more sufficient O₂ arrive on the surface of electrodes, which means higher conversion and faster diffusion kinetics for the catalyst. The corresponding K-L plots (Figure 6d) show an approximate linear relationship at different potentials, indicating the first-order reaction kinetics for ORR. The numbers of electron transfer for different samples during the ORR pathway are given in Figure 6e. The n values of Ag-MnFe₂O₄/NPG, Ag-MnFe₂O₄/SPG, and Ag-MnFe₂O₄/NSPG are calculated to be 3.08~3.21, 3.11~3.23, and 3.69~3.85, respectively. Thus, it indicates an available four electron pathway for Ag-MnFe₂O₄/NSPG.

**Figure 7.** The half-wave potential (vs. RHE) for ORR of different catalysts reported in references.

In addition, the OER performances of Ag-MnFe₂O₄/NPG, Ag-MnFe₂O₄/SPG, Ag-MnFe₂O₄/NSPG and Pt/C were studied in O₂-saturated 0.1 M KOH electrolyte with a scanning rate of 1600 rpm (Figure 6f). Prior to the onset of OER, Ag-MnFe₂O₄ nanoparticles have a redox peak in the region of 1.3~1.6 V (vs. RHE). The potential of Ag-MnFe₂O₄/NSPG at the current density of 10 mA·cm⁻² (E_j = 10) is 1.79 V, which is better than Ag-MnFe₂O₄/NPG (1.91 V), Ag-MnFe₂O₄/SPG (1.82 V) and Pt/C (1.97 V). Thus, the corresponding overpotential of Ag-MnFe₂O₄/NSPG is 560 mV, much smaller than Pt/C (740 mV). Ag-MnFe₂O₄/NSPG also demonstrates good OER catalytic performances.

To investigate the durability and methanol crossover effect of Ag-MnFe₂O₄/NSPG and Pt/C, chronoamperometric tests were carried out in O₂-saturated 0.1 M KOH. As shown in Figure 8a, Ag-MnFe₂O₄/NSPG catalyst displays 13.2% decay after 15,000 s, while Pt/C shows 29.1% decay. Current versus time (I-t) plots along with methanol addition are shown in Figure 8b. As 5 mL methanol is added into electrolyte at 400 s, the ORR current of Ag-MnFe₂O₄/NSPG has no significant change, indicating that Ag-MnFe₂O₄/NSPG catalyst has high catalytic selectivity for methanol. In comparison, Pt/C shows sharp current change due to the oxidation of methanol. It demonstrates the better methanol tolerance of Ag-MnFe₂O₄/NSPG.

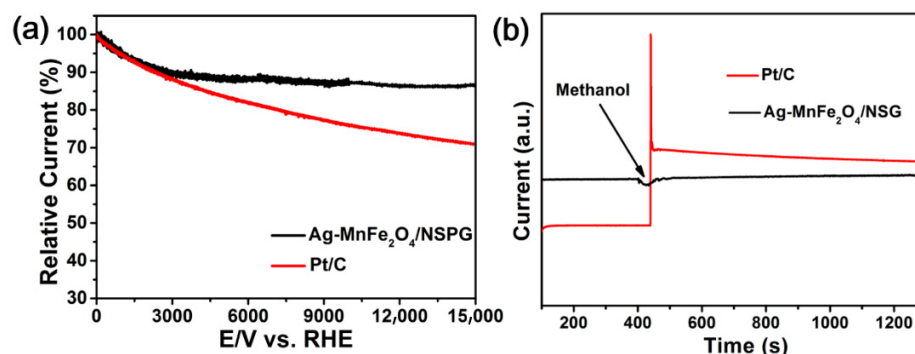


Figure 8. (a) Chronoamperometric response and (b) durability assessment of Ag-MnFe₂O₄/NSPG.

3. Experimental Section

3.1. Chemical Reagents and Materials

Nafion (5%), ferric acetylacetonate (99%), manganic acetylacetonate (99%), silver acetate (99%), melamine (99%), and 1-dodecanol (98%) were purchased from Sigma-Aldrich. Oleic acid (90%) and oleylamine (80%) were obtained from Aladdin. Phytic acid (50% in water) was obtained from Macklin. Dibenzyl disulfide (98%) was purchased from Beantown Chemical. 20 wt.% Pt/C was purchased from Hesen.

3.2. Material Synthesis

Synthesis of Ag-MnFe₂O₄ NPs. Ag-MnFe₂O₄ nanoparticles (NPs) were synthesized as reported [32]. Then, 1.0 mL oleic acid, 1.0 mL oleylamine, and 10 mL 1-dodecanol were mixed with stirring and heated to 220 °C. Then, 120 mg silver acetate was added and reacted for 1 h. The mixture was then cooled down to 200 °C. Next, 120 mg ferric acetylacetonate and 60 mg manganic acetylacetonate were subsequently added and reacted for another 1 h. The mixture was heated up to 220 °C and reacted 2 h. Finally, the mixture was cooled to room temperature. Products were collected and washed three times with ethanol.

Synthesis of NPG/SPG/NSPG. NPG, SPG, and NSPG were synthesized by similar route to NG [30]. Graphene oxide (GO) was synthesized by the Hummers' method [33]. Then, 100 mg GO was dispersed in 100 mL deionized water with ultra-sonication for 4 h to achieve a uniform solution. Then, 50 mg melamine and 50 mL phytic acid were slowly added into the dispersion. After 1 h ultra-sonication, the suspension was maintained under stirring at 90 °C for 2 h. After centrifugation with water, the precipitate was freeze-dried under vacuum. Finally, the powder was calcinated at 700 °C for 4 h at a heating rate of 5 °C min⁻¹ with a flow of Ar gas, denoted as NPG. SPG and NSPG were also synthesized with similar routes except for the replacement of melamine with 50 mg dibenzyl disulfide for SPG, 25 mg melamine and 25 mg dibenzyl disulfide for NSPG, respectively.

Synthesis of Ag-MnFe₂O₄/NPG, Ag-MnFe₂O₄/SPG and Ag-MnFe₂O₄/NSPG. Ag-MnFe₂O₄ NPs (8 mg) and doped graphene (16 mg) were dispersed in 24 mL toluene with stirring. After 16 h, solid materials were collected and washed with water for three times. The obtained materials were dried at room temperature and labeled as Ag-MnFe₂O₄/NPG, Ag-MnFe₂O₄/SPG and Ag-MnFe₂O₄/NSPG nanocomposites.

3.3. Material Characterizations

Transmission electron microscopy (TEM), X-ray diffraction (XRD), X-ray photoelectron spectroscopic (XPS), and Raman analyses of the samples were carried out as reported [30]. The content of nanoparticles in Ag-MnFe₂O₄/NSPG was determined by dissolving 0.25 g nanocomposite in 20 mL 5.0% HNO₃ solution for 2 h at room temperature and another 6 min at 80 °C, and then diluted to 100 mL with ultrapure water. Finally, elemental concentrations were measured by PerkinElmer Avio 200 ICP-OES.

3.4. Electrochemical Measurements

Ink of catalyst sample including 4.0 mg catalyst powder, 1.0 mg carbon black, 800 μL water, 200 μL isopropanol, and 20 μL Nafion (5%) was ultrasonicated for 1 h. Then, 3 μL ink was pipetted onto a glassy carbon disk. The ORR and OER performances were then studied with the rotating disk electrode (RDE) technique using the ALS RRDE-3A and CHI 760D system as reported [30].

4. Conclusions

In summary, heterojunction Ag-MnFe₂O₄ nanoparticles have been synthesized and supported on various doped graphenes, including NPG, SPG, and NSPG. Among these composites, Ag-MnFe₂O₄/NSPG demonstrate superior ORR and OER electrocatalytic performances, excellent durability and methanol resistance. ORR half-wave potential of Ag-MnFe₂O₄/NSPG reaches 0.831 V, which exceeds that of commercial Pt/C (0.827 V). When the OER current density is 10 mA·cm⁻², the potential of Ag-MnFe₂O₄/NSPG is 1.79 V, which also exceeds that of Pt/C (1.97 V). The multi-doping also stabilizes the loading of metal particles, so that Ag-MnFe₂O₄/NSPG shows good methanol resistance and excellent durability. After 14,000 s, the current loss is only reduced by 13.2%, much lower than that of Pt/C (29.1%). This indicates that metal particles/doped graphene composites have great application potentials and good prospects in metal-air batteries.

Author Contributions: H.D. and Y.C. designed the experiments and wrote the article; C.G., L.S. and Q.S. performed the experiments and analyzed the data; K.L. and L.D. designed the experiments. All authors have read and agreed to the published version of the manuscript.

Funding: This work was supported by the National Natural Science Foundation of China (21905153). Additionally, L. F. Dong thanks financial support from the Malmstrom Endowed Fund at Hamline University.

Conflicts of Interest: The authors declare no conflict of interest.

References

1. Wang, M.; Wang, W.; Qian, T.; Liu, S.; Li, Y.; Hou, Z.; Goodenough, J.B.; Ajayan, P.M.; Yan, C. Oxidizing vacancies in nitrogen-doped carbon enhance air-cathode activity. *Adv. Mater.* **2019**, *31*, 1803339. [[CrossRef](#)] [[PubMed](#)]
2. Shi, F.; He, J.; Zhang, B.; Peng, J.; Ma, Y.; Chen, W.; Li, F.; Qin, Y.; Liu, Y.; Shang, W.; et al. Plasmonic-enhanced oxygen reduction reaction of silver/graphene electrocatalysts. *Nano Lett.* **2019**, *19*, 1371–1378. [[CrossRef](#)] [[PubMed](#)]
3. Thaheem, I.; Kim, K.J.; Lee, J.J.; Joh, D.W.; Jeong, I.; Lee, K.T. High performance Mn_{1.3}Co_{1.3}Cu_{0.4}O₄ spinel based composite cathodes for intermediate temperature solid oxide fuel cells. *J. Mater. Chem. A* **2019**, *7*, 19696–19703. [[CrossRef](#)]
4. Santori, P.G.; Speck, F.D.; Cherevko, S.; Firouzjaie, H.A.; Peng, X.; Mustain, W.E.; Jaouen, F. High performance FeNC and Mn-oxide/FeNC layers for AEMFC cathodes. *J. Electr. Soc.* **2020**, *167*, 134505. [[CrossRef](#)]
5. Ratso, S.; Walke, P.R.; Mikli, V.; Ločs, J.; Šmits, K.; Vītola, V.; Šutka, A.; Kruusenberg, I. CO₂ turned into a nitrogen doped carbon catalyst for fuel cells and metal–air battery applications. *Green Chem.* **2021**, *23*, 4435–4445. [[CrossRef](#)]
6. Kaare, K.; Yu, E.; Käämbre, T.; Volperts, A.; Dobeles, G.; Zhurinsk, A.; Niaura, G.; Tamasauskaitė Tamasiunaite, L.; Norkus, E.; Kruusenberg, I. Biomass-derived Graphene-like Catalyst Material for Oxygen Reduction Reactio. *ChemNanoMat* **2021**, *7*, 307–313. [[CrossRef](#)]
7. Ratso, S.; Zitolo, A.; Käärik, M.; Merisalu, M.; Kikas, A.; Kisand, V.; Rahn, M.; Paiste, P.; Leis, J.; Sammelselg, V.; et al. Non-precious metal cathodes for anion exchange membrane fuel cells from ball-milled iron and nitrogen doped carbide-derived carbons. *Renew. Energy* **2021**, *167*, 800–810. [[CrossRef](#)]
8. Qu, L.; Liu, Y.; Baek, J.B.; Dai, L. Nitrogen-doped graphene as efficient metal-free electrocatalyst for oxygen reduction in fuel cells. *ACS Nano*. **2011**, *4*, 1321–1326. [[CrossRef](#)]
9. Liang, J.; Jiao, Y.; Jaroniec, M.; Qiao, S.Z. Sulfur and nitrogen dual-doped mesoporous graphene electrocatalyst for oxygen reduction with synergistically enhanced performance. *Angew. Chem. Int. Edit.* **2012**, *51*, 11496–11500. [[CrossRef](#)]
10. Wang, X.; Wang, J.; Wang, D.; Dou, S.; Ma, Z.; Wu, J.; Tao, L.; Shen, A.; Ouyang, C.; Liu, Q.; et al. One-pot synthesis of nitrogen and sulfur co-doped graphene as efficient metal-free electrocatalysts for the oxygen reduction reaction. *Chem. Commun.* **2014**, *50*, 4839–4842. [[CrossRef](#)]
11. Liu, Z.; Nie, H.; Yang, Z.; Zhang, J.; Jin, Z.; Lu, Y.; Xiao, Z.; Huang, S. Sulfur-nitrogen co-doped three-dimensional carbon foams with hierarchical pore structures as efficient metal-free electrocatalysts for oxygen reduction reactions. *Nanoscale* **2013**, *5*, 3283–3288. [[CrossRef](#)]
12. Wang, S.; Zhang, L.; Xia, Z.; Roy, A.; Chang, D.W.; Baek, J.B.; Dai, L. BCN graphene as efficient metal-free electrocatalyst for the oxygen reduction reaction. *Angew. Chem. Int. Edit.* **2012**, *51*, 4209–4212. [[CrossRef](#)]

13. Kumatani, A.; Miura, C.; Kuramochi, H.; Ohto, T.; Wakisaka, M.; Nagata, Y.; Ida, H.; Takahashi, Y.; Hu, K.; Jeong, S.; et al. Chemical dopants on edge of holey graphene accelerate electrochemical hydrogen evolution reaction. *Adv. Sci.* **2019**, *6*, 1900119. [[CrossRef](#)]
14. Zhang, N.; Liu, F.; Xu, S.; Wang, F.; Yu, Q.; Liu, L. Nitrogen-phosphorus co-doped hollow carbon microspheres with hierarchical micro-meso-macroporous shells as efficient electrodes for supercapacitors. *J. Mater. Chem. A* **2017**, *5*, 22631–22640. [[CrossRef](#)]
15. Yang, S.; Peng, L.; Huang, P.; Wang, X.; Sun, Y.; Cao, C.; Song, W. Nitrogen, phosphorus, and sulfur co-doped hollow carbon shell as superior metal-free catalyst for selective oxidation of aromatic alkanes. *Angew. Chem. Int. Edit.* **2016**, *55*, 4016–4020. [[CrossRef](#)]
16. Zhang, X.; Lu, Z.; Xu, G.; Wang, T.; Ma, D.; Yang, Z.; Yang, L. Single Pt atom stabilized on nitrogen doped graphene: Co oxidation readily occurs via the tri-molecular Eley-Rideal mechanism. *Chem. Phys.* **2015**, *17*, 20006–20013. [[CrossRef](#)]
17. Zhang, Y.; Fugane, K.; Mori, T.; Niu, L.; Ye, J. Wet chemical synthesis of nitrogen-doped graphene towards oxygen reduction electrocatalysts without high-temperature pyrolysis. *J. Mater. Chem.* **2012**, *22*, 6575. [[CrossRef](#)]
18. Zhang, X.; Lu, Z.; Fu, Z.; Tang, Y.; Ma, D.; Yang, Z. The mechanisms of oxygen reduction reaction on phosphorus doped grapheme. *J. Power Sour.* **2015**, *276*, 222–229. [[CrossRef](#)]
19. Razmjooei, F.; Singh, K.P.; Song, M.; Yu, J. Enhanced Electrocatalytic activity due to additional phosphorous doping in nitrogen and sulfur-doped graphene: A comprehensive study. *Carbon* **2014**, *78*, 257–267. [[CrossRef](#)]
20. Riel, A.M.S.; Jessop, M.J.; Decato, D.A.; Massena, C.J.; Nascimento, V.R.; Berryman, O.B. Experimental investigation of halogen-bond hard-soft acid-base complementarity. *Acta Crystallogr.* **2017**, *73*, 203–209. [[CrossRef](#)]
21. Talluri, B.; Thomas, T. Indications of hard-soft-acid-base interactions governing formation of ultra-small ($r < 3$ nm) digestively ripened copper oxide quantum-dots. *Chem. Phys. Lett.* **2017**, *685*, 84–88. [[CrossRef](#)]
22. Wang, Z.; Jin, H.; Meng, T.; Liao, K.; Meng, W.; Yang, J.; He, D.; Xiong, Y.; Mu, S. Fe, Cu-coordinated ZIF-derived carbon framework for efficient oxygen reduction reaction and zinc-air batteries. *Adv. Funct. Mater.* **2018**, *28*, 1802596. [[CrossRef](#)]
23. Lee, S.H.; Kim, J.; Chung, D.Y.; Yoo, J.M.; Lee, H.S.; Kim, M.J.; Mun, B.S.; Kwon, S.G.; Sung, Y.E.; Hyeon, T. Design principle of Fe-N-C electrocatalysts: How to optimize multimodal porous structures. *J. Am. Chem. Soc.* **2019**, *141*, 2035–2045. [[CrossRef](#)]
24. Geng, H.; Guo, Y.; Ding, X.; Wang, H.; Zhang, Y.; Wu, X.; Jiang, J.; Zheng, J.; Yang, Y.; Gu, H. Porous cubes constructed by cobalt oxide nanocrystals with graphene sheet coatings for enhanced lithium storage properties. *Nanoscale* **2016**, *8*, 7688–7694. [[CrossRef](#)]
25. Kumar, K.; Canaff, C.; Rousseau, J.; Clacens, S.A.; Kokoh, B. Effect of the oxide-carbon heterointerface on the activity of Co_3O_4 /NRGO nanocomposites toward ORR and OER. *J. Phys. Chem.* **2016**, *120*, 7949–7958. [[CrossRef](#)]
26. Qiu, B.; Deng, Y.; Du, M.; Xing, Y.; Zhang, J. Ultradispersed cobalt ferrite nanoparticles assembled in graphene aerogel for continuous photo-Fenton reaction and enhanced lithium storage performance. *Sci. Rep.* **2016**, *6*, 29099. [[CrossRef](#)]
27. Zou, J.; Kim, F. Diffusion driven layer-by-layer assembly of graphene oxide nanosheets into porous three-dimensional macrostructures. *Nat. Commun.* **2014**, *5*, 5254. [[CrossRef](#)]
28. Yu, S.; Webster, R.D.; Zhou, Y.; Yan, X. Novel carboxylated graphene oxide-CuS-Ag nanocomposite glass coating for organic degradation under solar light. *J. Chem. Technol. Biotechnol.* **2017**, *92*, 2626–2634. [[CrossRef](#)]
29. Chen, Y.; Li, Z.; Zhu, Y.; Sun, D.; Liu, X.; Xu, L.; Tang, Y. Atomic Fe dispersed on N-doped carbon hollow nanospheres for high-efficiency electrocatalytic oxygen reduction. *Adv. Mater.* **2019**, *31*, 1806312. [[CrossRef](#)]
30. Chen, Y.; Shi, Z.; Li, S.; Feng, J.; Pang, B.; Yu, L.; Zhang, W.; Dong, L. N, S-codoped graphene supports for Ag-MnFe₂O₄ nanoparticles with improved performance for oxygen reduction and oxygen evolution reactions. *J. Electroanal. Chem.* **2020**, *860*, 113930. [[CrossRef](#)]
31. Zhu, Y.; Cao, C.; Jiang, W.; Yang, S.; Hu, J.; Song, W.; Wan, L. Nitrogen, phosphorus and sulfur co-doped ultrathin carbon nanosheets as a metal-free catalyst for selective oxidation of aromatic alkanes and the oxygen reduction reaction. *J. Mater. Chem.* **2016**, *4*, 18470–18477. [[CrossRef](#)]
32. Chen, Y.; Liu, S.; Shi, Z.; Yu, J.; Dong, H.; Qin, Y.; Yu, L.; Dong, L. Effect of electronic coupling on the electrocatalytic performance of Ag-MFe₂O₄ (M = Co, Mn) nanocomposites. *J. Electrochem. Soc.* **2017**, *164*, F1483–F1488. [[CrossRef](#)]
33. Hummers, W.S., Jr.; Offeman, R.E. Preparation of graphitic oxide. *J. Am. Chem. Soc.* **1958**, *80*, 1339. [[CrossRef](#)]